Characterization and Physical Properties of Polymethylphenylsilsesquioxane (PMPSQ) and Hydroxyl-Functionalized Polystyrene (PS–OH) Hybrids

Seungpyo Hong,[1] Soon Man Hong,[1] Seung Sang Hwang,[1] Byoung Chul Kim[2]

[1]*Polymer Hybrids Research Center, Korea Institute of Science and Technology, P. O. Box 131, Cheongryang, 136-791, Seoul, South Korea*
[2]*Division of Chemical Engineering, Hanyang Univiersity, 17 Haingdang Dong, Seongdong Gu, 130-650, Seoul, South Korea*

Received 25 July 2002; accepted 2 April 2003

ABSTRACT: Polymethylphenylsilsesquioxane (PMPSQ–OH) and trimethylsilyl end-blocked PMPSQ (PMPSQ–EC) were prepared. The thermal decomposition behavior of these polymers was studied by thermogravimetric analysis (TGA) and FT-Raman spectroscopy. Hydroxyl-functionalized polystyrene (PS–OH) was also prepared by anionic living polymerization. Thin hybrid films of PMPSQ/PS–OH with various blend ratios were obtained by spin-coating on freshly cleaned glass. The surface morphology of the hybrid films was investigated by atomic force microscopy (AFM). In 80/20 PMPSQ/PS–OH hybrid film, the PS–OH component produced a very uniformly dispersed phase. This hybrid film contained small domains of PS–OH whose size ranged from 60 to 80 nm. As the content of PS–OH was increased, the domain morphology coarsened and phase inversion took place around 50 wt %. In the phase-inversed system, the PMPSQ-rich phase was uniformly distributed in the PS–OH-rich continuous phase. In addition, temperature-dependent dielectric properties of PMPSQ/PS–OH hybrids were investigated. Relaxation of the hybrids was observed with an increasing content of the PS–OH component due to the amorphous glass transition behavior of PS–OH. © 2003 Wiley Periodicals, Inc. J Appl Polym Sci 90: 2801–2812, 2003

INTRODUCTION

Since ladderlike polyphenylsilsesquioxane (PPSQ) was reported by Brown et al.,[1] a number of researchers have studied the synthesis of polysilses–quioxanes (PSSQs) with a ladder structure and PSSQ-based blends.[2–4] The silicone ladder polymers have proven to be very useful and widely applicable in industrial fields due to their excellent thermal stability, low moisture absorption, high modulus, good transparency, and low dielectric constant. One of the most attractive advantages of the PSSQ is its extremely good thermal stability. However, little literature on the thermal decomposition behavior of PSSQ has been published.

In the last two decades, organic/inorganic hybridization has been extensively studied as an alternative to the conventional complicated method to make hybrid materials.[5–8] PSSQ-based organic/inorganic blends have been investigated to be used as microelectronic packaging insulators, optical devices, and coating materials.[9–13] Recently, organic/inorganic hybridization studies have been aimed to obtain nanoscaled hybrid materials.[13,14] The properties of a hybrid material depend not only on the properties of the individual components, but also on the phase morphology and interfacial properties of the hybrid. The organic dispersed inorganic matrix might be favorably exploited in developing new technologies such as nanofoaming, nanotemplating, and microlithographic patterning. It would also be useful in developing nanodevices such as optical waveguides and cladding material in optical fibers because of the excellent optical transparency and low refractive index of the inorganic matrix. We reported earlier on the phase-separation behavior of PPSQ and polystyrene (PS) hybrid materials from this point of view.[15]

In this study, polymethylphenylsilsesquioxane (PMPSQ–OH) was prepared and modified to trimethylsilyl end-blocked PMPSQ (PMPSQ–EC). PMPSQ was initially designed to obtain some synergistic effect in the physical properties of PPSQ and polymethylsilsesquioxane (PMSQ). The thermal decomposition behavior of two polymers with different end groups was studied to investigate the effect of the end group on the thermal decomposition of the polymers. In addition, it is important to study the surface morphology of the PMPSQ-containing thin hybrid films because it determines the phase-separation behavior, polymer–air interface phenomena, wettability, and

Correspondence to: S. M. Hong (smhong@kist.re.kr).

Journal of Applied Polymer Science, Vol. 90, 2801–2812 (2003)

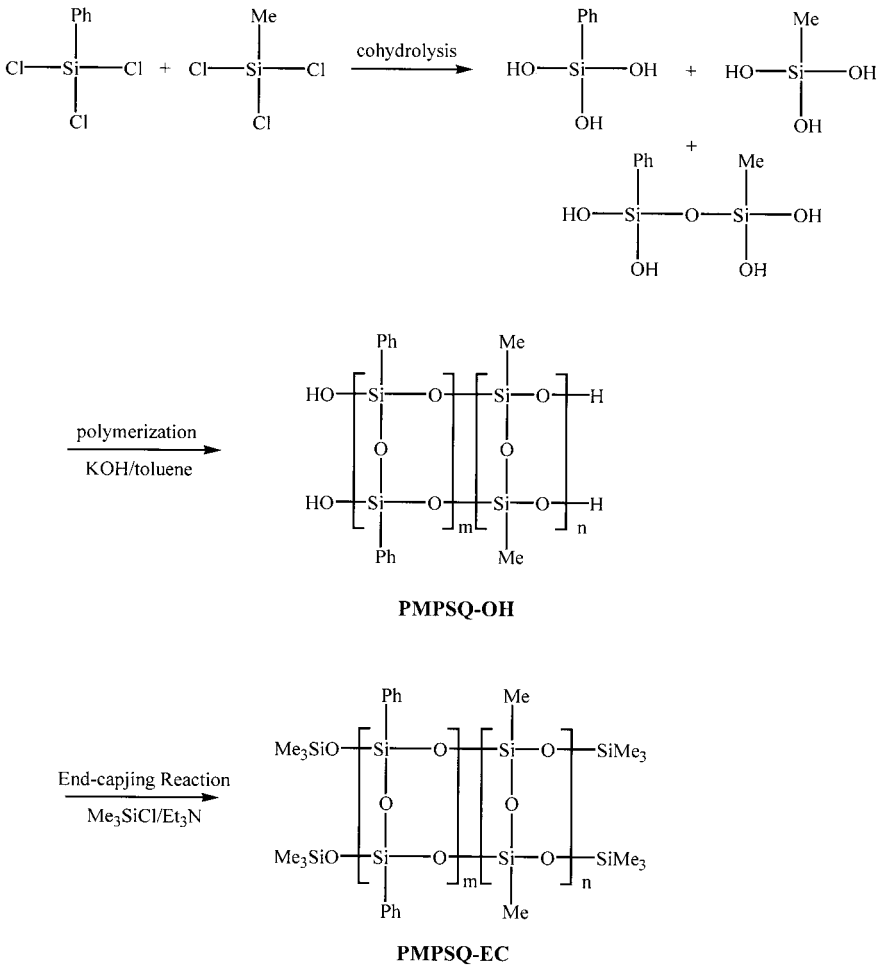

Scheme 1 Synthesis of PMPSQ–OH and PMPSQ–EC.

adhesion on glass substrates, etc. In this respect, we investigated the phase-separation behavior of PMPSQ/hydroxyl-functionalized polystyrene (PS–OH) hybrids at various compositions. Temperature-dependent dielectric properties of the hybrids are also discussed.

EXPERIMENTAL

Preparation of polymers

Potassium hydroxide (KOH) from Aldrich was used as a catalyst for preparation of PMPSQ without further purification. Toluene was distilled over sodium metal before use. PMPSQ was synthesized by the method previously described in our articles.[16–20] A mixture of phenyltrichlorosilane and methyltrichlorosilane with a molar ratio of 1/1 was hydrolyzed below 0°C for 3 h. The initial hydrolysate of the reaction mixture obtained was then dissolved in toluene with a small amount of KOH. The solution was heated to the reflux temperature and stirred for 16 h. The obtained product was then filtered and dried in a vacuum oven at 110°C for 12 h. A silanol capping reaction was carried out as described in our earlier literature.[17,19] The synthetic route of PMPSQ–OH and PMPSQ–EC is shown in Scheme 1. PS–OH was prepared by anionic polymerization of PS followed by introduction of a hydroxyl group on the chain end using ethylene oxide as shown in Scheme 2.[15]

^{1}H-NMR ($CDCl_3$): δ 7.4–6.3 (aromatic protons), 3.3 (—CH_2OH), 2.3–0.8 (backbone CH_2) ppm.

Identification of polymers

^{1}H-NMR spectra were obtained using a Varian Gemini-200 spectrometer with $CDCl_3$ as an internal standard. The M_n and molecular weight distribution (MWD) were determined by gel permeation chromatography (GPC). The analyzer was composed of a Shimadzu LC-10A pump, a Shodex RI SE-31 detector, a Shimadzu C-R7A Chromatopac data processor, a Shodex DEGAS KT-16 degasser, and a Sugai U-620 column oven. A combination of two PS gel columns of Tosoh TSK gel G4000H_8 and G2500H_8 was used with chloroform as the eluent at 35°C. Its limited exclusion

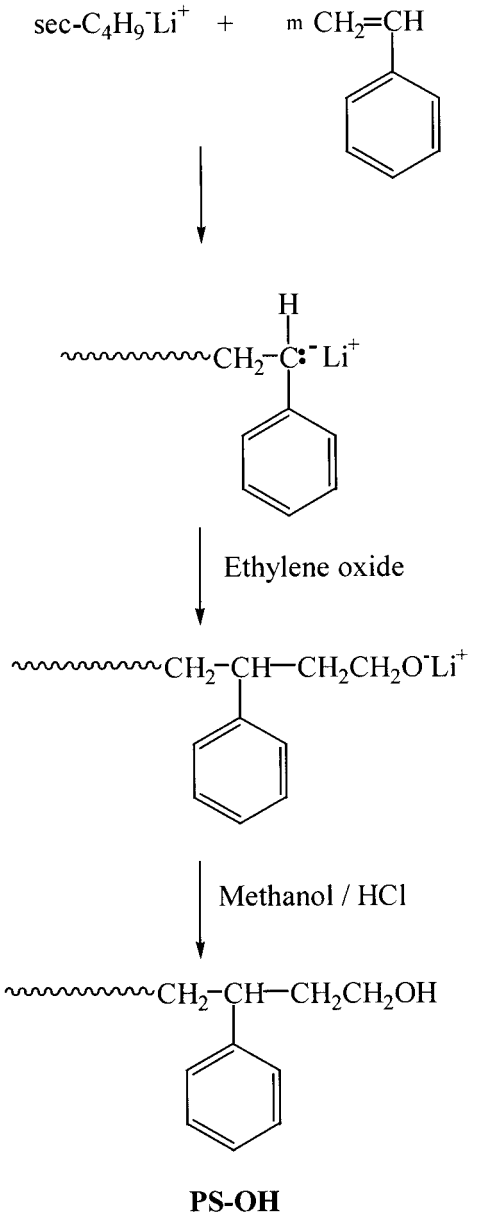

Scheme 2 Synthesis of hydroxyl-functionalized PS.

molecular weight was 7×10^5 Da. The molecular weight was calibrated by PS standards. Thermogravimetric analysis was measured with a TGA 2950 from DuPont Instruments Co. Temperature was increased to 800°C from the initial equilibrium temperature of 30°C. The heating rate was 10°C/min. FT-Raman spectra were recorded on a Perkin–Elmer System 2000 NIR FT-Raman spectrometer equipped with a Nd:YAG CW laser (λ = 1064 nm) source using the back-scattering method. FTIR spectra were measured on a Matson series 5000. DSC measurements were carried out at the heating rate of 20°C, after a first scan to avoid the thermal history of the hybrid materials. DSC thermograms were measured with a DSC 2910 from DuPont Instruments Co.

TABLE I
Prepared PMPSQ/PS–OH Hybrids at Various Compositions

Sample	Composition
1	Pure PMPSQ–OH
2	Pure PMPSQ–EC
3	PMPSQ–OH/PS–OH 80/20
4	PMPSQ–EC/PS–OH 80/20
5	PMPSQ–OH/PS–OH 50/50
6	PMPSQ–EC/PS–OH 50/50
7	PMPSQ–OH/PS–OH 20/80
8	PMPSQ–EC/PS–OH 20/80
9	Pure PS–OH

Specimen preparation and AFM measurement

PMPSQ–OH, PMPSQ–EC, and PMPSQs/PS–OH hybrids at different weight ratios were dissolved in toluene with a concentration of 15% by weight. The compositions of all samples are listed in Table I. Each solution was spin-coated on a freshly cleaned glass slide after filtering the solution through a Millipore Teflon filter (0.2 μm). The thickness of the prepared films was fixed at 1 μm. The films were first dried slowly at room temperature for 1 day. The films were then annealed at 100°C for 24 h under a nitrogen atmosphere and cooled to room temperature. Micrographs were recorded with a multimode scanning probe microscope (Digital Instruments, Inc.). The tapping-mode was used to obtain phase-imaging data with 125-μm-long cantilevers. The cantilever had a very small tip radius of 5–10 nm. The lateral scan frequency was about 1.0 Hz. The sample was moved in the x–y plane and voltage was applied, which moved the piezo driver over the z-axis, to keep the probing force constant, resulting in a three-dimensional height image of the sample surface.

Specimen preparation and measurement of dielectric properties

Aluminum (CERAC™ specialty inorganics with purity of 99.999%) electrodes were vaporized on a freshly cleaned glass slide using ULVAC VPC-260F vacuum-deposition equipment. End-capped PMPSQ and

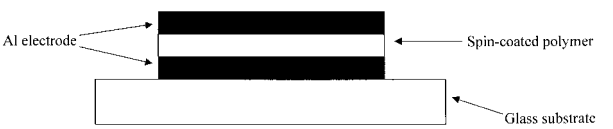

Scheme 3 Schematic diagram of prepared specimen for measurement of dielectric properties.

TABLE II
M_n and MWD of Prepared PMPSQ and PS–OH by GPC

Material	M_n	MWD
PMPSQ	11,000	1.26
PS–OH	5000	1.09

Calibrated by PS standards.

PMPSQ–EC/PS–OH hybrids, at different compositions, were dissolved in toluene with a concentration of 15% by weight. The solution was spin-coated on the aluminum-coated glass after filtering the solution through a Millipore Teflon filter (0.2 μm). The films were annealed at 100°C for 24 h under a nitrogen atmosphere and cooled to room temperature. Finally, aluminum electrodes were vaporized on the specimen. A simplified schematic diagram of the sample preparation is shown in Scheme 3.

Dielectric relaxation and dielectric constant measurements were carried out on a Hewlett–Packard LF impedance analyzer Model 4192A equipped with Mettler Toledo FP82HT hot stage and Mettler Toledo FP90 central processor. The temperature was increased to 100°C from an initial temperature of 30°C. The heating rate was 5°C/min at a frequency of 1 MHz.

RESULTS AND DISCUSSION

Preparation of polymers

The M_n and MWD of PMPSQ and PS–OH measured by GPC are listed in Table II. The M_n of PMPSQ and PS–OH are 11,000 and 5000, respectively. The MWD of PMPSQ and PS–OH are 1.26 and 1.09, respectively.

^{1}H-NMR spectra of PMPSQ–OH (sample 1) and PMPSQ–EC (sample 2) are shown in Figure 1. The broad peaks at 7.8–6.5 ppm are assigned to Si–Ph groups and peaks at 0.4 to −0.6 ppm are assigned for Si–Me groups. Si–OH groups are detected at 1.6–1.4 ppm as a very sharp peak in the PMPSQ–OH spectrum. The integration ratio of Si–Ph and Si–Me groups is 5/3, which indicates Si–Ph and Si–Me are evident with a molar ratio of 1/1. After the silanol capping reaction with trimethylsilyl chloride, a narrow and sharp $SiMe_3$ peak at 0.19 ppm is detected with disappearance of the Si–OH group peak. This result confirmed to us that all the silanol groups are converted to $SiMe_3$ groups without any unreacted silanol groups. Other identification and characterization of PMPSQ by ^{1}H-NMR, FT-Raman, FTIR, ^{29}Si NMR, and TGA were described in detail previously.[16,17] PS–OH was synthesized and characterized by thin-layer chromatography (TLC), FTIR, and GPC as shown in our earlier report.[15]

Thermal decomposition behavior of PMPSQs and PMPSQ–EC/PS–OH hybrids

Figure 2 shows the thermal decomposition behavior of samples 1 and 2. An initial decomposition temperature of sample 1 is observed at 150°C, probably because of a crosslinking condensation reaction between hydroxyl groups in the polymer chains ends. This reaction would lead to a reduction in weight of sample

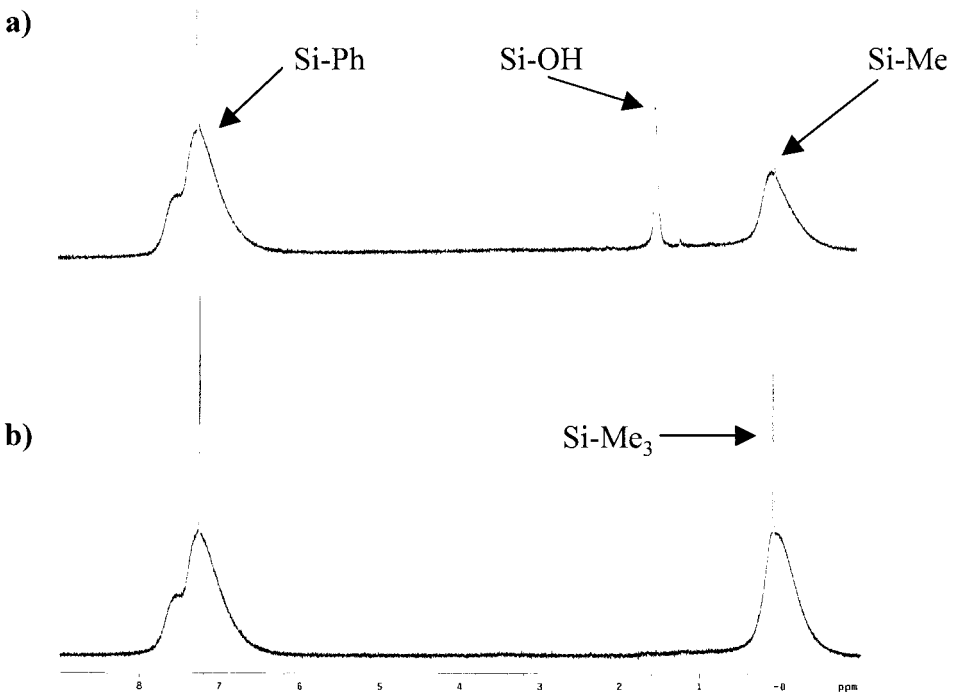

Figure 1 ^{1}H-NMR spectra of (a) PMPSQ–OH and (b) PMPSQ–EC.

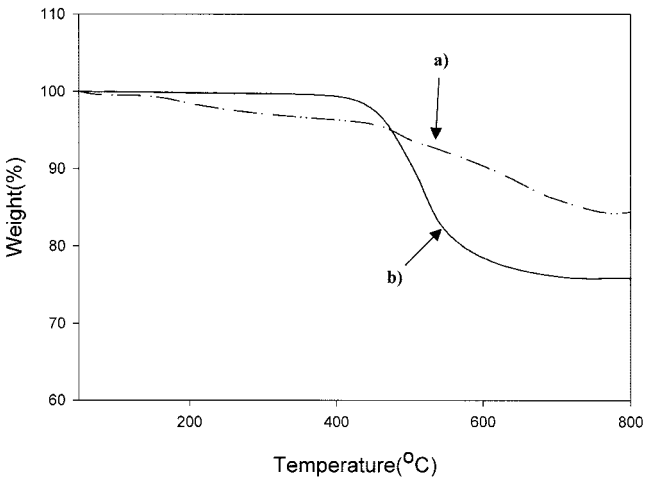

Figure 2 TGA thermograms of (a) PMPSQ–OH and (b) PMPSQ–EC.

1 of about 2–3 %. Sample 2 does not show any thermal transition behavior until 420°C, the initial decomposition temperature of sample 2, because no hydroxyl group exists in the polymer chains. Furthermore, thermal decomposition gradually occurs at 350–550°C in both cases. To investigate the thermal decomposition behavior focused on decomposing groups, samples were taken at various intermediate temperatures to measure FT-Raman spectroscopy as a quantitative method.

Figure 3 shows FT-Raman spectra of samples 1 and 2 at room temperature. Peaks at 3054, 1595, 1572, 1192, 1156, 1133, and 622 cm^{-1} are assigned to Si–Ph groups. Si–Me groups are observed at 2972, 2913, and 1411 cm^{-1}. Si—O—Si stretching is detected at 1000–1100 cm^{-1} as a double band. Peak areas of Si–Me groups of sample 2 are larger than that of sample 1 because Si–Me groups in trimethylsilyl end groups contribute to the increased peak intensity. The Si–Ph peak at 3054 cm^{-1} and Si–Me peaks at 2972 and 2913 cm^{-1}, normalized by the peak intensity of the Si—O—Si double band, are measured for quantitative analysis of the decomposition behavior as shown in Figure 4. As temperature increases, a noticeable reduction of Si–Ph and Si–Me groups is observed. Particularly, some difference in the thermal decomposition behavior between PMPSQ–OH and PMPSQ–EC is observed. Si–Ph and Si–Me groups in PMPSQ–OH are gradually decomposed at 350°C. However, those groups in PMPSQ–EC do not show any thermal decomposition at 350°C, probably because the trimethylsilyl end blocks protect the pendant groups from pyrolysis. Furthermore, the pyrolysis rate of the pendant groups in PMPSQ–EC is much slower than that of the groups in PMPSQ–OH. We suggest that this fact results from the effect of thermally stable end groups on the thermal decomposition. The peak area is calculated based on the Si—O—Si double band as a standard as shown in Table III. At temperatures above 550°C, the Si—O—Si peak intensity becomes so turbulent that quantitative analysis cannot be accurately carried out.

Figure 5 shows TGA thermograms of PMPSQ/PS–OH hybrid materials. As the content of PS–OH increases, the initial decomposition temperature of the samples is decreased. Furthermore, the weight of the thermally decomposed residue is increased with an increasing content of PMPSQ–EC, which is due to that the thermal stability of an inorganic polymer is much better than that of an organic polymer. Table IV shows the glass transition temperatures (T_g's) measured by DSC. With an increase in the PMPSQ content in the hybrid materials, the T_g's of the hybrids are increased by a maximum of 10°C. In addition, PMPSQ–OH-based hybrids show higher T_g's than those of the PMPSQ–EC-based hybrids, indicating that the T_g shift results from the larger increase in the polymer–polymer interaction.

Surface morphology of the thin hybrid films

Surface morphology of PMPSQ–OH thin film (sample 1), investigated by AFM, shows excellent film planarity without any defect and crack (not presented here). Phase-separation behaviors of samples 3 and 4 based

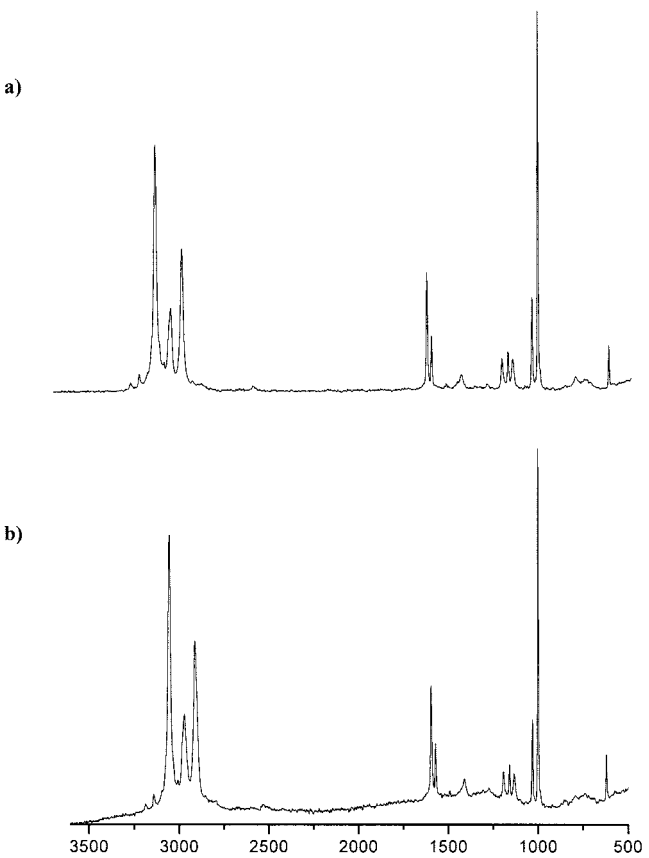

Figure 3 FT-Raman spectra of (a) PMPSQ–OH and (b) PMPSQ–EC at room temperature.

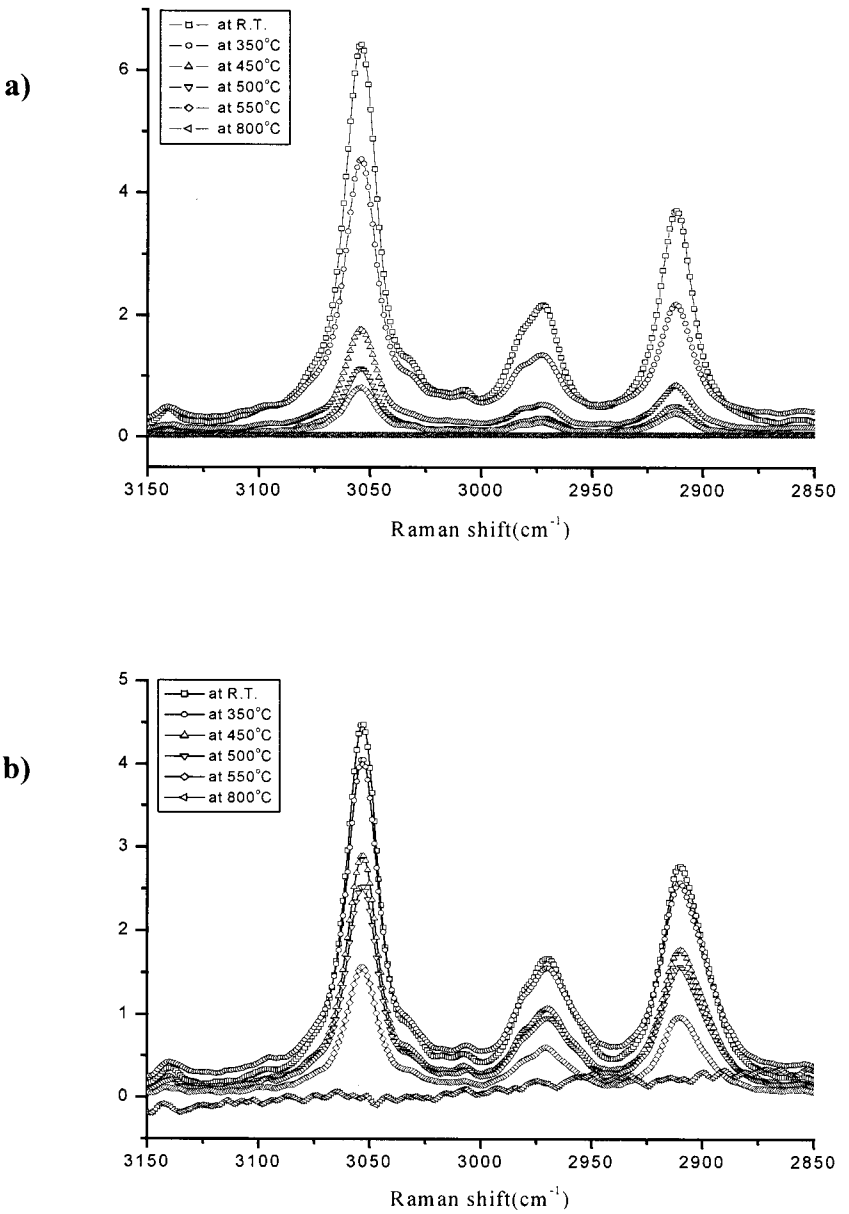

Figure 4 FT-Raman spectra of (a) PMPSQ–OH and (b) PMPSQ–EC normalized by peak area of the Si—O—Si double band.

on PMPSQ–OH, PMPSQ–EC, and PS–OH were investigated by AFM, as shown in Figures 6 and 7, respectively. Since the surface morphology of the thin hybrid films is strongly influenced by interactions between the polymer surface and air, the surface energy of the blend components is an important factor in determining the surface topography. In general, the polymer component with lower surface energy segregates preferentially to the air interface to minimize the polymer–air surface tension.[21,22] The surface tension was calcu-

TABLE III
Peak Area of FT-Raman Spectra with Si—O—Si Peak Area at 1000–1100 cm^{-1} as Standards

	Sample 1			Sample 2		
Temperature (°C)	Si—O—Si	Si–Ph	Si–Me	Si—O—Si	Si–Ph	Si–Me
Room temperature	1.00	1.45	1.28	1.00	1.79	1.85
350 °C	1.00	1.08	0.98	1.00	1.73	1.82
450 °C	1.00	0.54	0.53	1.00	1.54	1.35
500 °C	1.00	0.49	0.39	1.00	1.53	1.28
550 °C	1.00	0.38	0.32	1.00	0.89	0.92

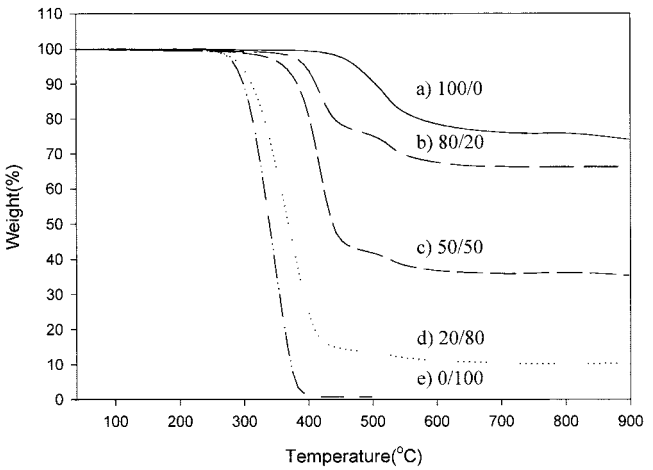

Figure 5 TGA thermograms of PMPSQ–EC/PS–OH hybrids.

lated from the contact angles of water and glycerol.[23] PMPSQs are assumed to have a lower surface energy (PMPSQ–OH; 30.34 mN m^{-1}, PMPSQ–EC; 28.70 mN m^{-1}) compared with PS–OH (31.04 mN m^{-1}). In consequence, the PS-rich phase is believed to protrude from the PMPSQ-rich one.[24] PMPSQ–OH has four hydroxyl groups in each chain end, which increase the degree of interaction of PMPSQ–OH and PS–OH through interhydroxyl interaction. Furthermore, aromatic groups in the polymer backbone also result in the increase of polymer–polymer interaction via aromatic–aromatic interaction. In the case of sample 3 (Fig. 6), well-dispersed PS–OH domains are obtained with the domain size of 60–80 nm. The PS–OH phase is uniformly distributed. Sample 4, however, shows a larger PS–OH phase (80–100 nm) as shown in Figure 7. This result comes from the decreased polymer–polymer interactions because PMPSQ–EC has no hydroxyl end groups. AFM images of samples 3 and 4 reveal that a more uniform phase distribution was observed with an increase of polymer–polymer interactions.

TABLE IV
Glass Transition Temperatures (T_g's) of the Hybrids Measured by DSC

Sample	T_g
1	—
2	—
3	91.33
4	88.27
5	87.86
6	86.92
7	85.17
8	85.19
9	81.22

As the content of the PS–OH component increases, however, distinct phase separation is observed. Figures 8 and 9 show AFM images of samples 5 and 6, respectively. In Figure 8, the PMPSQ–OH phase and the PS–OH phase are observed as cocontinuous phases. This result comes from the general rule that the same polymers tend to aggregate with each other. Two phases show self-aggregation due to their hydroxyl interaction between chain ends. Sample 5 was investigated to prove that self-aggregation occurs because of interaction between hydroxyl groups in each polymer chain end. Sample 6 shows a more regular PMPSQ–OH dispersed phase than that of sample 5 (Fig. 9). Reduced interactions, caused by an end-cap-

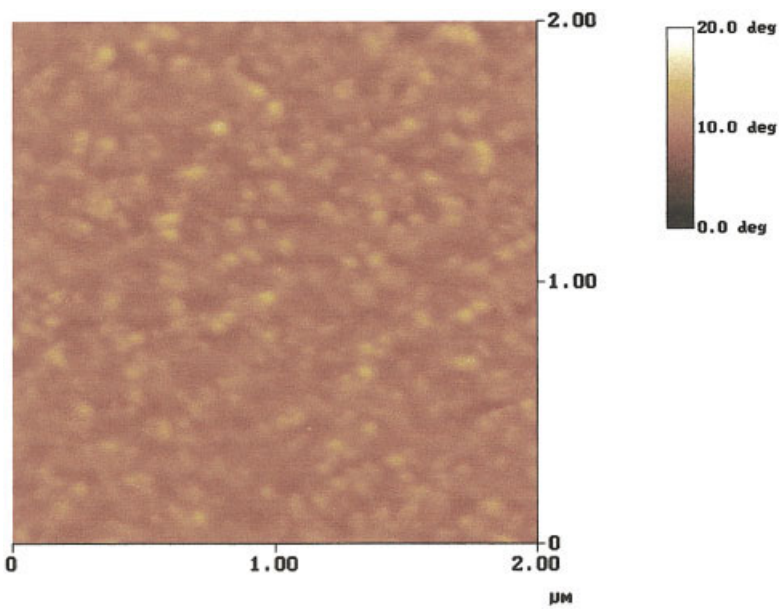

Figure 6 AFM images of PMPSQ–OH/PS–OH (80/20).

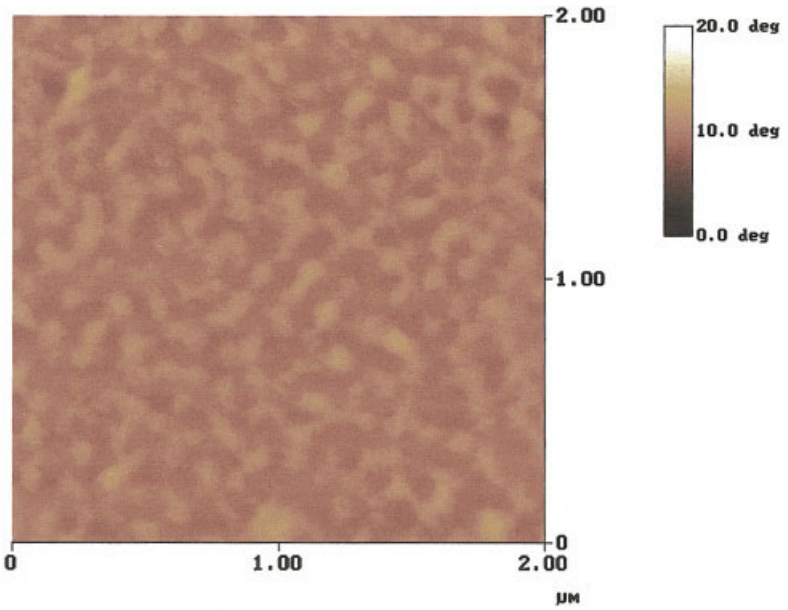

Figure 7 AFM images of PMPSQ–EC/PS–OH (80/20).

ping reaction of PMPSQ, leads to the noticeable domain formation of PS–OH. The domain size of the PS–OH phase in sample 6 is 150–400 nm.

AFM images of samples 7 and 8 are shown in Figures 10 and 11, respectively. The distinct domain formation of the PMPSQ-rich phase of the PMPSQ/PS–OH (20/80) hybrid system is observed. Sample 7 reveals that the PMPSQ–OH phase is distributed as a relatively regular form in the PS–OH-rich continuous phase. The domain size of the PMPSQ–OH phase is in the range from 50 to 70 nm. Figure 11 (sample 8) shows a similar tendency to that of Figure 10 (sample 7). The domain size of the PS–OH phase is in the range of 60–80 nm. Sample 8 also shows a more regular distribution of the PMPSQ–EC phase than that of sample 7. This result probably comes from self-aggregation at some critical weight ratio of PMPSQ–OH (around 50 wt %).

Below 50 wt %, of any composition of the two components for PMPSQs/PS–OH hybrid system, a well-dispersed phase, containing small and uniform domains in the continuous phase, is obtained with an increasing degree of interaction between the two con-

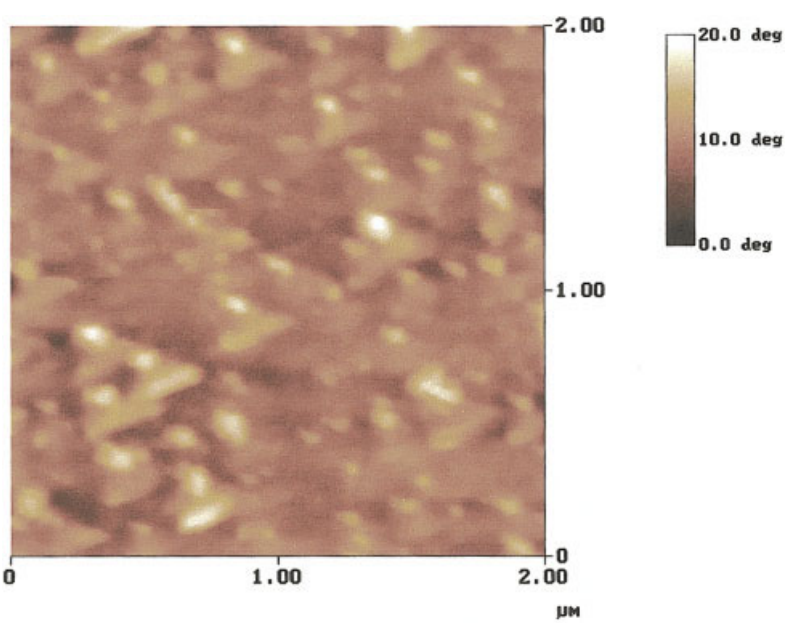

Figure 8 AFM images of PMPSQ–OH/PS–OH (50/50).

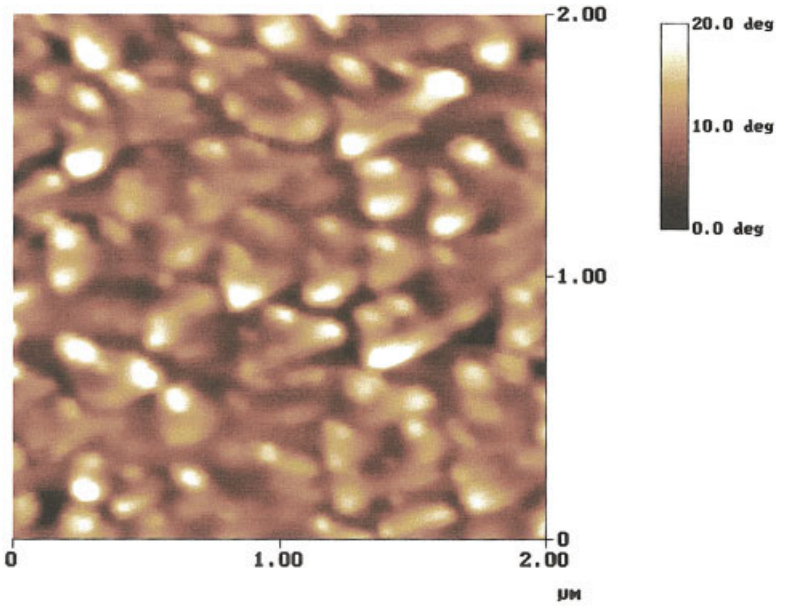

Figure 9 AFM images of PMPSQ–EC/PS–OH (50/50).

stituent polymers. As polymer–polymer interactions, such as interhydroxyl interactions and aromatic–aromatic interactions, increase, smaller and more regular domains are obtained in both cases of PMPSQ-dominant hybrids and PS–OH-dominant hybrids.

FTIR was used to examine possible interactions between the two components. The hydroxyl-absorption intensities of the two hybrid films are normalized on the basis of the C—H stretching absorption band for comparison, because the band should have the same intensity at the same content of PS–OH. The hybrid solution was cast onto a NaCl crystal window and dried at 100°C for 24 h in a vacuum oven before measuring the IR. To avoid hydrogen bonding between the polymer and moisture in the air, FTIR was measured immediately after the film was taken out of the oven and under a dried nitrogen atmosphere. Figure 12 shows FTIR spectra of the PMPSQ/PS–OH hybrids (samples 1–9). FTIR spectra of pure PMPSQ–OH and PS–OH were also taken for comparison. PMPSQ–OH exhibits a relatively sharp and weak hydroxyl absorption band centered at 3600 cm^{-1} and a broad absorption band centered at 3400 cm^{-1} , as shown in Figure 12(a). As the PS–OH content is increased, the hydroxyl absorption peak intensity becomes larger and broader. Particularly, the hydroxyl

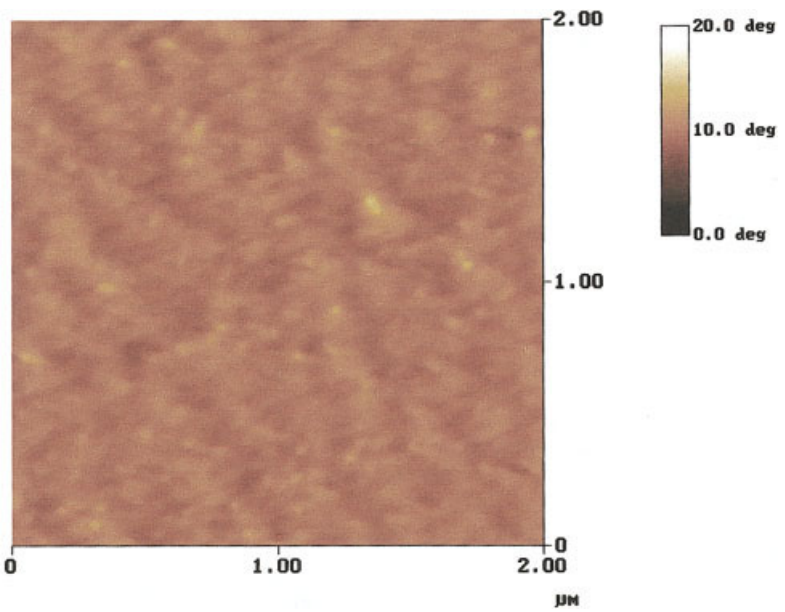

Figure 10 AFM images of PMPSQ–OH/PS–OH (20/80).

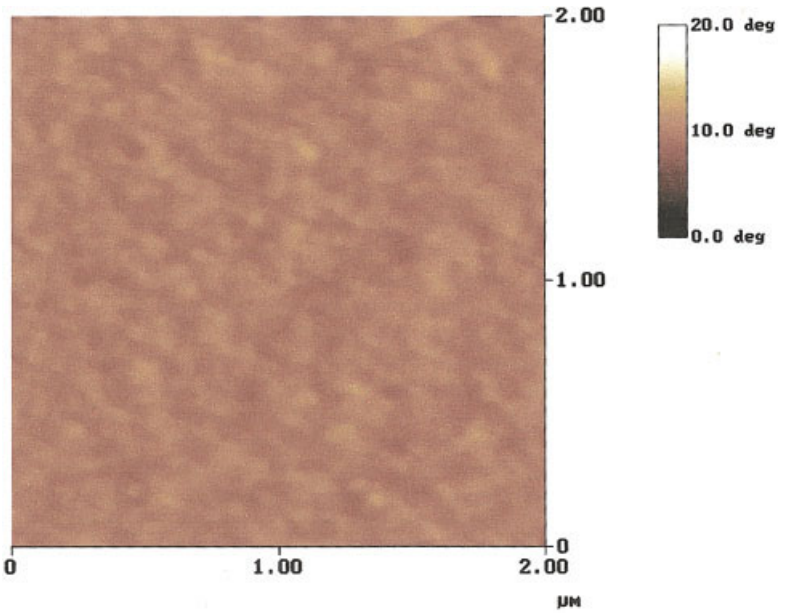

Figure 11 AFM images of PMPSQ–EC/PS–OH (20/80).

absorption peak becomes the largest and broadest in the PMPSQ–OH/PS–OH (50/50) hybrid, sample 5. This result is probably because the interhydroxyl interaction between the two polymers and self-hydroxyl interaction occur simultaneously. It may result in self-aggregation of the two phases as mentioned for Figure 8. In the case of the PMPSQ–OH/PS–OH (20/80) hybrid film [Fig. 12(g)], hydroxyl absorption, however, is significantly reduced. This implies that the PS–OH dominant hybrid film shows little hydroxyl interaction but has phenyl–phenyl interaction, resulting in regular phase distribution and a relatively uniform domain size. We suggest that phenyl–phenyl interaction enhances phase distribution in the case of PS–OH dominant hybrids. Consequently, good phase distribution in the continuous matrix (samples 4, 7, and 8) would come from a phenyl–phenyl interaction as described in earlier literature.[25]

To confirm this, we compared the IR data of the PMPSQ–OH/PS–OH (samples 1, 3, 5, and 7) and PMPSQ–EC/PS–OH hybrids (samples 2, 4, 6 and 8). We found that PMPSQ–OH/PS–OH hybrid films exhibit an interhydroxyl interaction while PMPSQ–EC/PS–OH films show little interhydroxyl interaction from these spectra. In particular, it is obvious that sample 5 shows a very broad and large absorption band centered at 3400 cm^{-1}, which results in self-aggregation. In contrast, sample 6 shows little interhydroxyl interaction, resulting in no self-aggregation in the AFM measurement [Fig. 12(e,f)]. Accordingly, the FTIR spectra of PMPSQ–OH/PS–OH

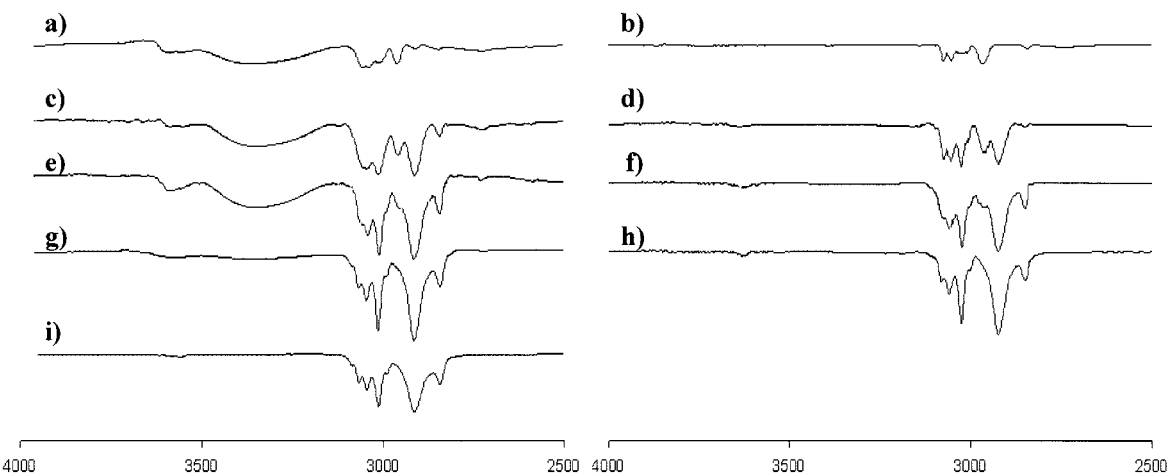

Figure 12 FTIR spectra of (a) sample 1, (b) sample 2, (c) sample 3, (d) sample 4, (e) sample 5, (f) sample 6, (g) sample 7, (h) sample 8, and (i) sample 9.

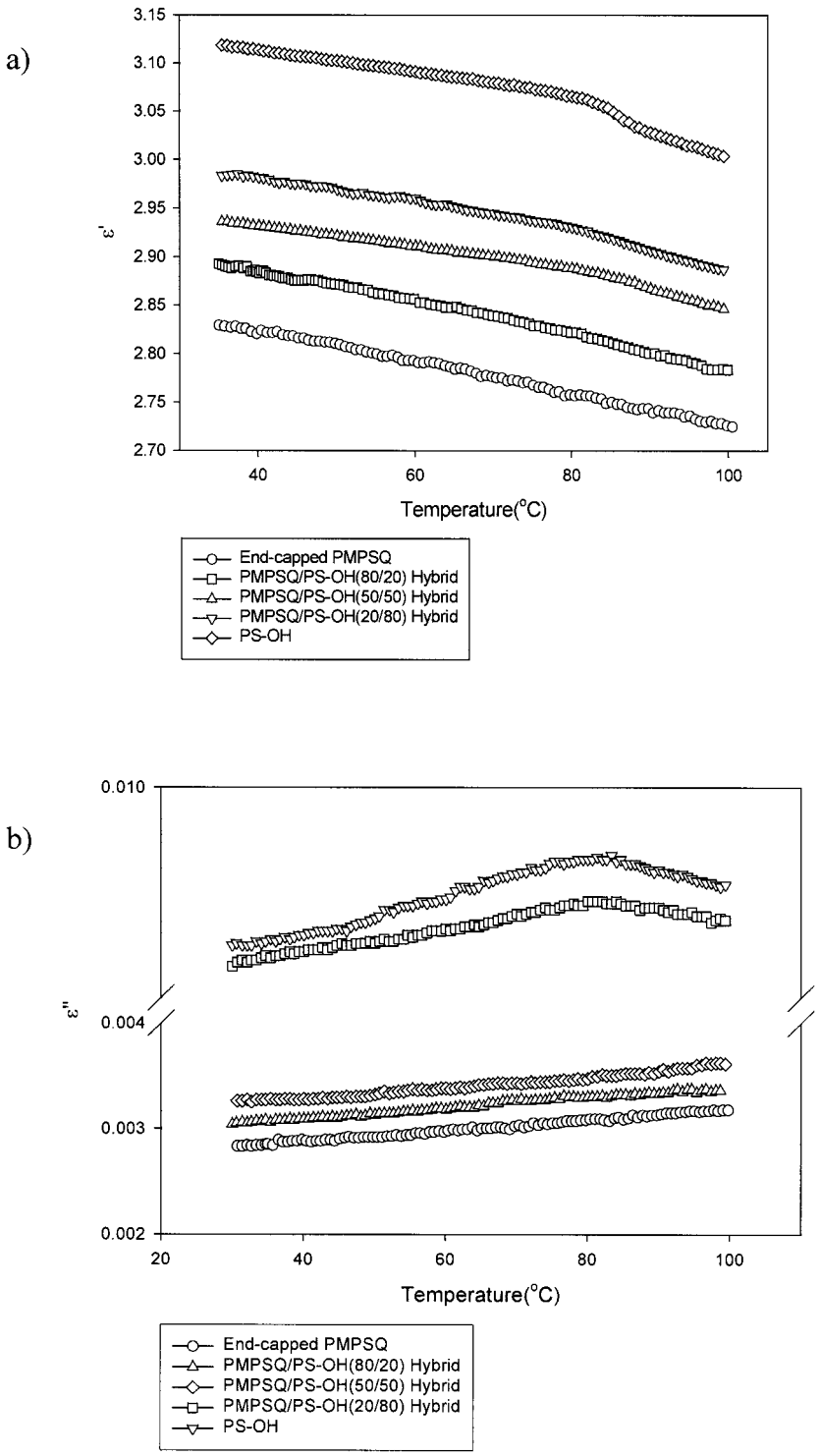

Figure 13 (a) Dielectric constants and (b) dielectric loss of thin hybrid films. The loss curves are displaced for clarity.

hybrid films show good agreement with the AFM measurement.

Measurement of dielectric properties of the thin hybrid films

Dielectric constants of PMPSQ–EC/PS–OH hybrid samples over the range from 30 to 100°C are shown in Figure 13(a). As the measuring temperature increased to 100°C, the PMPSQ–EC/PS–OH material goes through a transition in the dielectric behavior around the glass transition temperature (T_g) of PS–OH (about 80°C) in the PS–OH dominant hybrids. All the measured hybrid materials exhibit temperature-dependent dielectric constants. The di-

electric constant, ε', was calculated from the capacitance according to

$$\varepsilon' = \frac{c\,l}{\varepsilon_0\,A} \quad (1)$$

where ε_0 is the dielectric constant of the vacuum state, 8.854×10^{-12} F/m; c, the capacitance of the thin films; l, the film thickness; and A, the area of the Al electrode. The dielectric constants of the hybrids are increased with increase in the PS–OH component. The dielectric constants of samples 2, 4, 6, 8, and 9 at 60°C at 1 MHz are 2.79, 2.85, 2.91, 2.96, and 3.09, respectively.

Plots of the dielectric loss (ε'') against the temperature at 1 MHz for the PMPSQ–EC/PS–OH hybrid samples are shown in Figure 13(b). Ionic conduction phenomena are not observed over the temperature range of 20–100°C. It should be noted that the dielectric loss curves are shifted vertically to avoid overlap in the plots. The dielectric loss for PMPSQ-dominant hybrid films is negligible, <0.0003, under all conditions investigated. These phenomena result from the thermal stability and the rigidity of the inorganic PMPSQ, which enervates chain mobility. This indicates that the inorganic polymer has little influence on the dielectric loss and, presumably, on the rotational motions of the benzene rings in the PS–OH chain. On the other hand, the dielectric loss of the PMPSQ/PS–OH hybrid with the PS–OH-rich phase exhibits a broad maximum around 80°C. This peak is due to the amorphous glass transition relaxation of PS–OH.[26]

CONCLUSIONS

PMPSQ–OH and PMPSQ–EC, with highly regulated chemical structures, were prepared to investigate the effect of end groups on the thermal decomposition behavior. A quantitative analysis of pyrolysis was investigated by FT-Raman spectroscopy. A distinct difference in the thermal decomposition behavior between PMPSQ–OH and PMPSQ–EC was observed. The trimethylsilyl end block enhances the thermal stability of the pendant groups (Si–Ph and Si–Me groups) in the polymer. AFM images revealed the nanoscaled phase-separation behavior between PMPSQ and PS–OH. A well-dispersed PS–OH phase on the continuous PMPSQ phase is observed in the PMPSQ/PS–OH (80/20) hybrid. An increased interaction between two polymers results in smaller and more regular domain distributions. FTIR also reveals interhydroxyl interaction between PMPSQ–OH and PS–OH hybrid films. As the PS–OH content increases, however, each hydroxyl group preferentially tends to form hydroxyl bonding with itself, not with each other. Thus, for PMPSQ–EC-based hybrids, only a π–π interaction occurred, with a polymer having a PS–OH content over 50 wt % exhibiting better phase distribution. The dielectric constant of the films is increased with increase of the PS–OH component ratio. Dielectric loss occurs in the PS–OH-rich hybrid film due to an amorphous glass transition relaxation.

The authors thank Dr. Hyoung-Jun Kim for assistance with the AFM measurements. Thanks are also extended by the authors to Dr. Dong Young Kim for assistance with the FT-Raman spectrometer measurements.

References

1. Brown, J. F., Jr.; Vogt, L. H., Jr.; Katchman, A.; Eustance, J. W., Kiser, K. M.; Krantz, K. W. J Am Chem Soc 1960, 82, 6194.
2. Brown, J. F., Jr. J Polym Sci C 1963, 1, 83.
3. Li, G. Z.; Yamamoto, T.; Nozaki, K.; Hikosaka, M. Polymer 2000, 41, 2827.
4. Li, G.; Jin, Y.; Shi, L.; Ye, M.; Bai, F. J Polym Sci Part B Polym Phys 1996, 34, 1079.
5. Dislich, H. Angew Chem Int Ed Engl 1971, 10, 363.
6. Yoldas, B. E. J Mater Sci 1979, 14, 1843.
7. Mackenzie, J. D. J Non-Cryst Solids 1982, 48, 1.
8. Brinker, C. J.; Scherer, G. W. J Non-Cryst Solids 1985, 70, 301.
9. Shirai, S.; Kanbe, J.; Ohno, S. U.S. Patent 4 405 702, 1983.
10. Haddad, T. S.; Lichtenhan, J. D. Macromolecules 1996, 29, 7302.
11. Sellinger, A.; Laine, R. M. Macromolecules 1996, 29, 2327.
12. Tsuchida, A.; Bolln, C.; Sernetz, F. G.; Frey, H.; Mülhaupt, R. Macromolecules 1997, 30, 2818.
13. Mascia, L.; Kioul, A. J Mater Sci Lett 1994, 13, 641.
14. Morikawa, A. Polym J 1992, 28, 107.
15. Kim, D. W.; Hwang, S. S.; Hong, S. M.; Lee, E. C. Polym J 2000, 32, 531.
16. Hwang, S. S.; Hong, S. M.; Lee, E. C.; Hong, S. P. Jpn. Patent 13-149 443, 2001, pending.
17. Hong, S. P.; Lee, E. C.; Hong, S. M.; Hwang, S. S.; Kim, B. C., submitted for publication in Angew Chem.
18. Lee, E. C.; Kimura, Y. Polym J 1997, 29, 678.
19. Lee, E. C.; Kimura, Y. Polym J 1998, 30, 234.
20. Lee, E. C.; Kimura, Y. Polym J 1998, 30, 730.
21. Walheim, S.; Böltau, M.; Mlynek, J.; Krausch, G.; Steiner, U. Macromolecules 1997, 30, 4995.
22. Tanaka, K.; Takahara, A.; Kajiyama, T. Macromolecules 1996, 29, 3232.
23. Van Krevelen, D. W. Properties of Polymers; Elsevier: New York, 1990.
24. Owens, D. K.; Wendt, R. C. J Appl Polym Sci 1969, 13, 1741.
25. Tamaki, R.; Samura, K.; Chujo, Y. Chem Commun 1998, 1131.
26. Huo, P.; Cebe, P. Macromolecules 1992, 25, 902.